Experimental observation of controllable kinetic constraints in a cold atomic gas

M. M. Valado,[1,2] C. Simonelli,[1,2] M. D. Hoogerland,[3] I. Lesanovsky,[4] J. P. Garrahan,[4] E. Arimondo,[1,2,5]
D. Ciampini,[1,2,5] and O. Morsch[1,2]

[1]*Dipartimento di Fisica "E. Fermi," Università di Pisa, Largo Bruno Pontecorvo 3, 56127 Pisa, Italy*

[2]*INO-CNR, Via G. Moruzzi 1, 56124 Pisa, Italy*

[3]*Department of Physics, University of Auckland, Private Bag 92019, Auckland, New Zealand*

[4]*School of Physics and Astronomy, University of Nottingham, Nottingham NG7 2RD, United Kingdom*

[5]*CNISM UdR Dipartimento di Fisica "E. Fermi," Università di Pisa, Largo Pontecorvo 3, 56127 Pisa, Italy*

Many-body systems relaxing to equilibrium can exhibit complex dynamics even if their steady state is trivial. In situations where relaxation requires highly constrained local particle rearrangements, such as in glassy systems, this dynamics can be difficult to analyze from first principles. The essential physical ingredients, however, can be captured by idealized lattice models with so-called kinetic constraints. While so far constrained dynamics has been considered mostly as an effective and idealized theoretical description of complex relaxation, here we experimentally realize a many-body system exhibiting manifest kinetic constraints and measure its dynamical properties. In the cold Rydberg gas used in our experiments, the nature of the kinetic constraints can be tailored through the detuning of the excitation lasers from resonance. The system undergoes a dynamics which is characterized by pronounced spatial correlations or anticorrelations, depending on the detuning. Our results confirm recent theoretical predictions, and highlight the analogy between the dynamics of interacting Rydberg gases and that of certain soft-matter systems.

Complex collective relaxation in many-body systems is often accompanied by a dramatic slowdown of diffusion processes and the emergence of nonergodic and glassy phases [1–4]. At low temperatures or high densities their evolution is often dominated by steric hindrances affecting particle motion. Local rearrangements are highly constrained, giving rise to collective—and often slow—relaxation. These features can be seen to be the consequence of effective kinetic constraints in the dynamics [5]. A kinetic constraint is a condition on the rate for a local transition dependent on the local environment: The transition and its reverse—irrespective of whether they are energetically favorable or unfavorable—can only occur if the constraint is satisfied. Kinetic constraints [6] can severely restrict relaxation in situations where local particle arrangements make satisfying them unlikely, which is typical of fluid systems with excluded volume interactions such as dense colloids or supercooled liquids [1–4]. When a constraint is satisfied, however, the transition is allowed and a local rearrangement is "facilitated" [5,6]. Kinetic constraints naturally give rise [7] to collective and spatially heterogeneous relaxation, and are used to describe situations where the correlation properties of the dynamics go beyond those of the static stationary state, a salient feature of glassy systems [4].

Steric hindrances and dynamic facilitation are argued to play a central role in the behavior of glass formers [5]. However, it can be difficult [8] to establish unambiguously the relation between microscopic processes and emerging kinetic constraints, or between idealized models with explicit kinetic constraints and actual physical systems. In this Rapid Communication we establish such a direct connection by reporting the experimental observation of correlated many-body excitation dynamics in a strongly interacting Rydberg gas [9–12] whose origin lies in explicit kinetic constraints that can be theoretically derived from the quantum-mechanical equations of motion of the system.

We explore two kinds of kinetic constraints which lead to the suppression or the facilitation of atomic excitations in the vicinity of atoms excited to Rydberg states. Our experimental technique allows us to measure both the mean number of excitations and the fluctuations around the mean as a function of time, and we find clear signatures of the constraints in the pronounced (anti)correlations evident in both quantities. The experimental observations are in excellent agreement with numerical simulations of a kinetically constrained system of Ising spins, where the constraint is explicitly derived from the actual interatomic interactions.

The kinetic constraints and resulting correlated excitation processes explored in this Rapid Communication are shown schematically in Fig. 1. The relevant internal (electronic) dynamics of the Rydberg atoms can be modeled in terms of pseudo Ising spins having a (noninteracting) ground state $|g\rangle$ (spin down) and an excited state $|r\rangle$ (spin up) coupled by a Rabi frequency Ω. Atoms at positions r_i and r_j in the Rydberg state $|r\rangle$ interact through the van der Waals interaction $V_{ij} = \frac{C_6}{|r_i - r_j|^6}$, where C_6 is the van der Waals interaction coefficient [13,14] (which, in the present experiment, is positive). Here, we explore the regime of incoherent evolution, $\gamma \gg \Omega$, where γ is the decay rate of the atomic coherences. In this strong dissipation limit the evolution of the many-body system is restricted to the subspace of classical spin configurations by virtue of the quantum Zeno effect [15]. The dynamics can be written as a classical rate equation with rates for excitation and deexcitation [9,11],

$$\Gamma_i(\Delta) = \frac{\Omega^2}{2\gamma}\left[1 + \left(\frac{\Delta - \frac{1}{\hbar}\sum_{i \neq j} V_{ij} n_j}{\gamma}\right)^2\right]^{-1}, \quad (1)$$

where $n_j = 1$ if the atom at position r_j is in the Rydberg state and 0 otherwise. Generally, therefore, the excitation rate
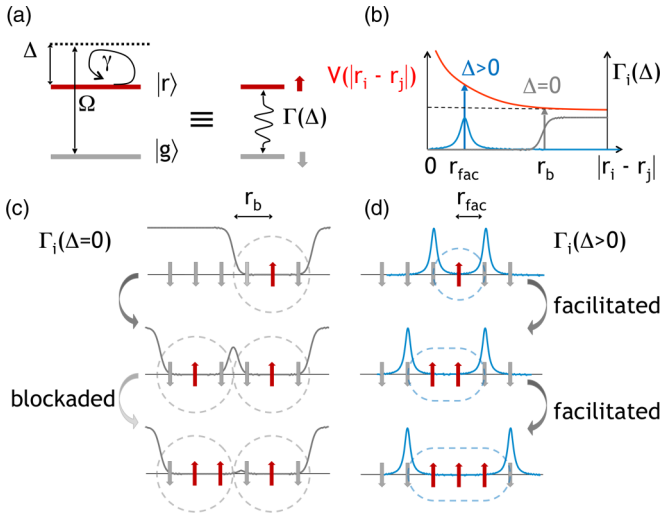
FIG. 1. Kinetic constraints realized in a gas of Rydberg atoms. (a) Schematic representation of the laser-induced coupling between ground and Rydberg states with Rabi frequency Ω and detuning Δ, where coherence between the atomic states is lost at a rate γ. Each atom can be effectively described as an Ising pseudospin. In the incoherent regime $\gamma \gg \Omega$, the dynamics of an atom reduces to incoherent state changes (spin flips) at a rate $\Gamma_i(\Delta)$. (b) Interaction potential $V(|r_i - r_j|)$ between two excited atoms at positions r_i and r_j (red line) and excitation rates $\Gamma_i(\Delta)$ for $\Delta > 0$ (blue line) and $\Delta = 0$ (gray line). The excitation rate for $\Delta = 0$ drops to zero for interatomic distances $|r_i - r_j|$ below the blockade radius r_b (*blockade constraint*), whereas it peaks at the facilitation radius r_{fac} for $\Delta > 0$ (*facilitation constraint*). This leads to blockaded dynamics, shown in (c), and to facilitated dynamics, shown in (d), respectively. In (c), excitation of individual atoms occurs at the resonant rate until the distance between adjacent excitations approaches the blockade radius. The third spin from the left is excited at a strongly reduced rate as it is located within the blockade radius. In (d), a seed excitation enables further excitations at the facilitation distance r_{fac}.

$\Gamma_i(\Delta)$ for an atom depends on the state of all the atoms in its vicinity and on the detuning Δ of the excitation laser from resonance. For the resonant case $\Delta = 0$ (in practice, $\Delta \ll \gamma$), the interactions between an atom and its neighbors lead to a *blockade constraint* resulting in anticorrelated dynamics [9,16]: The more excited atoms there are in the vicinity, the smaller Γ_i, leading to a spatially inhomogeneous local excitation rate and an overall slowing down of the relaxation process as the number of excitations in the systems grows. The interparticle distance below which this blockade constraint becomes important is given by the (incoherent) blockade radius $r_b = (C_6/\hbar\gamma)^{\frac{1}{6}}$. By contrast, for $\Delta > 0$ the off-resonant single-atom excitation rate is small, but now a *facilitation constraint* appears [10]: An excited atom somewhere in the system shifts atoms contained within a shell of radius r_{fac} and width δr_{fac} into resonance, where $r_{fac} = (C_6/\hbar\Delta)^{\frac{1}{6}}$, which corresponds to the van der Waals interaction compensating the laser detuning [12,17–22], and $\delta r_{fac} = \frac{r_{fac}}{6\Delta}\gamma$. We will show that this leads to strikingly different features in the excitation dynamics in comparison to the case of resonant excitation.

In our experiments the conditions of Fig. 1 are realized with magneto-optical traps (MOTs) of ^{87}Rb atoms that are excited

to repulsively interacting $70S$ Rydberg states [23]. The roughly spherical atomic clouds have a Gaussian density profile with widths between 45 and 160 μm and contain between 10^4 and 1.2×10^6 atoms at typical temperatures around 150 μK. We control the (effective) number of atoms and hence the density of the clouds (keeping their size and shape constant) by depumping a fraction of the atoms in the $F = 2$ hyperfine ground state to the $F = 1$ state using a resonant laser pulse of duration up to 2 μs (for details, see Ref. [24]). This state lies 6.8 GHz below the $F = 2$ state (the ground state for the Rydberg excitation process) and hence does not couple to the Rydberg excitation lasers. After the depumping pulse, we infer the effective atom number by exciting a few Rydberg atoms (less than 10, in order to avoid interaction effects) on resonance and measuring the total growth rate, which in the noninteracting, incoherent regime is proportional to the atom number. Excitation to the $70S$ Rydberg state (for which $C_6 = h \times 869.7$ GHz μm^6) is achieved by a two-photon process with laser beams near 420 nm (waist 10 or 40 μm) and 1013 nm (waist 110 μm), and the 420 nm laser detuned by 660 MHz from the $6P_{3/2}$ excited state. Depending on the sizes and propagation directions of those beams, we can realize two geometries: an effective one-dimensional (1D) geometry, in which the 420 nm laser is focused to a waist of around 10 μm (comparable to the blockade and facilitation radii) and the 1013 nm intersects the 420 nm beam and the atomic cloud at a 45° angle; and a three-dimensional (3D) geometry, in which the 420 nm laser has a waist of 40 μm and copropagates with the 1013 nm laser. The combined decoherence rate due to the laser linewidths and residual Doppler broadening is estimated to be $\gamma = 2\pi \times 0.7$ MHz. After an excitation pulse of up to 100 μs, the Rydberg atoms are field ionized and detected by a channeltron with an overall detection efficiency η of around 40%. The experiments are repeated 100 times for each set of parameters in order to obtain the mean number and variance.

We simulate the dynamics of our laser-driven Rydberg gas in the limit of strong dissipation using the equation [15] $\dot{v} = \sum_i \Gamma_i(|r_i\rangle\langle g_i| + |g_i\rangle\langle r_i| - |r_i\rangle\langle r_i| - |g_i\rangle\langle g_i|)v$, where v encodes the probability of the system to be in one of its classical configurations (products of the local spin states $|r_i\rangle$ and $|g_i\rangle$). In order to account for the inhomogeneity of the atomic cloud we distributed the atomic positions according to a Gaussian profile in close approximation to the experimental situation. The spatially inhomogeneous laser profile was accounted for by using a locally varying Rabi frequency for the calculation of the value of the rate function Γ_i for each individual atom. In the simulation only atoms inside an effective excitation volume V_{exc} were considered. This excitation volume was defined as the region in which the free flipping rate of an atom was at least 10% (3D data) or 5% (1D data) of the maximum rate. The simulations where conducted by implementing a classical kinetic Monte Carlo algorithm, and the results were averaged over 1000 runs (1D data) or 100 runs (3D data). In the simulations the residual thermal motion of the atoms (average velocity around 120 nm μs^{-1} for a MOT temperature of 150 μK) is neglected.

We now proceed to investigate the nonequilibrium dynamics of our system under the action of the two constraints introduced above. As a first step we set $\Delta = 0$, thus realizing the *blockade constraint*, and verify that the dynamics of our
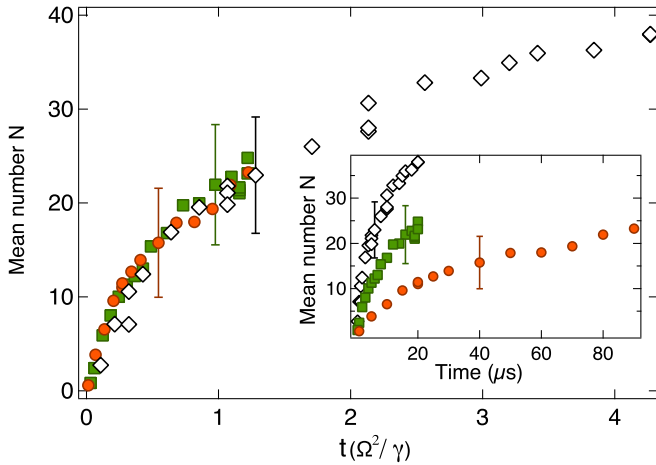
FIG. 2. Dependence of incoherent dynamics on the Rabi frequency for resonant excitation. The inset shows the mean number of excitations in a sample of 7×10^5 atoms in a MOT of width 60 μm in the 3D configuration as a function of time for three different Rabi frequencies: $\Omega/2\pi = 81$ (open diamonds), 43 (green squares), and 20 kHz (red circles). When multiplying the excitation times by Ω^2/γ (where $\gamma/2\pi = 0.7$ MHz), the three curves collapse onto each other (main figure), demonstrating the expected Ω^2 scaling in the incoherent excitation regime. Representative error bars are one standard deviation of the mean (s.d.m.).

system is incoherent and hence in the regime of validity of the above rate equation. We do this by measuring the resonant excitation dynamics, represented by the mean number of excitations N as a function of time t (here and in the rest of this Rapid Communication we report the derived actual quantities obtained by dividing the observed quantities by the detection efficiency η), for different values of the Rabi frequency Ω. In the regime of incoherent Rydberg excitation, where our experiments are conducted, the excitation rate Γ_i [Eq. (1)] is proportional to Ω^2/γ [22]. This is in contrast to the scaling proportional to Ω which is expected for a fully coherent excitation process [25]. Figure 2 shows the results of experiments for three different values of Ω. The experimental data plotted versus $t \cdot \Omega^2/\gamma$ collapse onto a single curve, demonstrating the expected scaling of the incoherent dynamics.

In order to systematically study the effect of the blockade constraint on the dynamics, we control the degree of correlation of our system by the number of atoms per blockade length $\frac{r_b}{a}$ [where $a = (\frac{V_{exc}}{N_g})^{\frac{1}{3}}$ is the mean distance between N_g ground-state atoms in the excitation volume V_{exc}, and $r_b = 11.1$ μm for our parameters]. We vary this quantity by changing the effective density of the MOT as described above (here, we use the 1D configuration in order to keep $N \lesssim 100$ and thus to avoid saturating our detection system). In this way, we can prepare samples with $\frac{r_b}{a}$ between around 1.3 (i.e., close to the noninteracting case $\frac{r_b}{a} \leq 1$) and $\frac{r_b}{a} = 4.2$. The results of these experiments are shown in Fig. 3(a), together with the results of the numerical simulation described above, that exhibit excellent qualitative and good quantitative agreement (to within overall factors between 0.5 and 2, indicated in the captions to Figs. 3 and 4, that allow for experimental
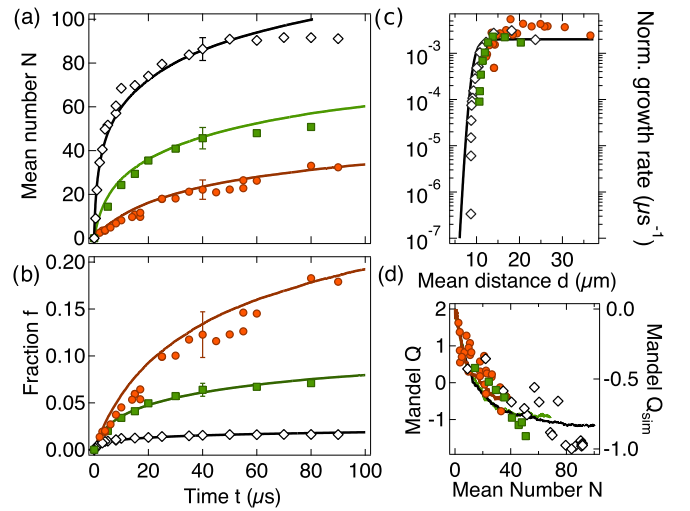

FIG. 3. Evidence for the blockade constraint in a gas of Rydberg atoms. (a) Mean number of excitations and (b) excitation fraction as a function of time for different atom numbers N_g inside the interaction volume: 5600 (open diamonds), 715 (green squares), and 180 (red circles). These correspond to values of the parameter $\frac{r_b}{a}$ of 4.2, 2.1, and 1.3, respectively. The numerical simulations (solid lines) have been scaled vertically by a factor of 1.8. (c) Normalized growth rate as a function of the mean distance d between excited atoms. The solid line is obtained from the expression for $\Gamma_i(\Delta)$ in a mean-field approach. (d) Mandel Q parameter as a function of mean excitation number. The vertical axis on the left corresponds to experimental data, and that on the right to the numerical simulation (solid lines). Representative error bars are one s.d.m.

uncertainties in the number of atoms, in the exact shape of the atomic cloud and in the intensity distributions of the lasers, as well as for effects due to residual thermal motion). The crossover between the initial excitation regime in which the
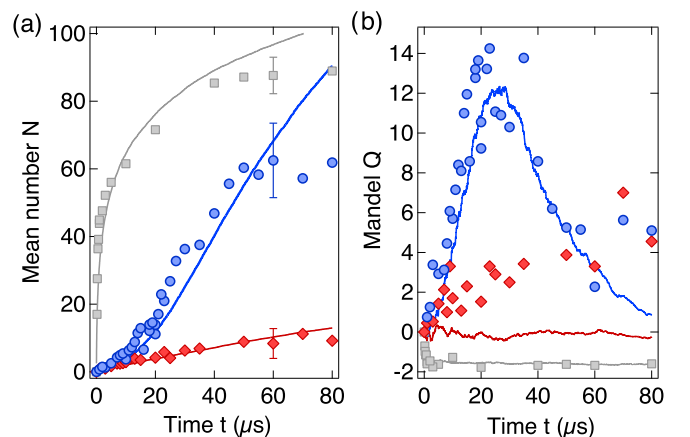

FIG. 4. Evidence for the facilitation constraint in a gas of Rydberg atoms. (a) Mean number of excitations as a function of time for $\Delta/2\pi = +19$ MHz (blue circles), $\Delta/2\pi = -19$ MHz (red diamonds), and $\Delta = 0$ (gray squares). The numerical simulations (solid lines) have been scaled vertically by a factor 0.56. Representative error bars are one s.d.m. (b) The Mandel Q parameter as a function of time. The numerical simulations (solid lines) have been scaled by a factor 2.

interactions play no role, reflected by a linear increase in N, and the blockade regime is clearly visible, indicating the point at which the average distance $d = (\frac{V_{exc}}{N})^{\frac{1}{3}}$ between excitations becomes smaller than r_b [26]. Figure 3(b) shows the fraction of excited atoms obtained by normalizing the data of Fig. 3(a) by the number of ground-state atoms N_g in the excitation volume. In the blockade regime the excited fraction levels off much more sharply for large values of $\frac{r_b}{a}$, which again demonstrates the action of the blockade constraint.

These results can be analyzed quantitatively through the average growth rate of excitations per atom $(dN/dt)/N_g$ as a function of d. The growth rate is extracted by numerically differentiating the N vs t data from Fig. 3(a) after smoothing them in order to avoid artifacts due to noisy data. We expect this rate to decrease abruptly when the mean distance d between excitations falls below r_b, which defines the effective range of influence of a Rydberg atom. This expectation is confirmed by Fig. 3(c), in which all the data sets follow a single curve which is flat for $d > r_b$ and decreases by four orders of magnitude between 11 and 6 μm. The theoretical curve in Fig. 3(c) was obtained from the expression for Γ_i ($\Delta = 0$) in a mean-field approach by averaging Ω^2 over the excitation volume defined above and substituting $|r_i - r_j|$ by half the mean distance between excitations, where the volume used for calculating the mean distance was chosen as 1.92×10^4 μm^3, which gave the best agreement with experiment. The interaction term in $\Gamma_i(\Delta)$ was multiplied by 6 in order to account for six nearest neighbors for each atom.

The strong correlations caused by the kinetic constraints are also expected to affect the fluctuations of the systems, which we investigate through the Mandel Q parameter [27]. Similarly to the dipole blockade in the coherent regime [28,29], the blockade constraint should lead to a negative Q parameter that decreases with the number of excitations since for large numbers the system has fewer choices for distributing the excitations, which in turn leads to reduced fluctuations. Moreover, following the above reasoning, the Q parameter should depend exclusively on the number of excitations and not on the number of ground-state atoms, so plotting Q as a function of N for all three data sets should yield a single curve. Again, this is experimentally confirmed in Fig. 3(d). The deviations of the experimental data from the simulation are most likely due to technical noise and fluctuations in the atom number, laser intensity and detuning (positive Q for small values of N), and saturation effects of the detection system (values of $Q < -1$ for large N).

In contrast to the blockade constraint, which causes a slowing down of the dynamics, the *facilitation constraint* should speed up the dynamics and lead to a bunching of excitations. In order to explore this regime, we now set $\Delta/2\pi = +19$ MHz, for which $r_{fac} = 6.4$ μm and $\delta r_{fac} = 39$ nm. Since we expect the predicted facilitation dynamics to be the more pronounced the larger the overall facilitation volume, which grows with an increasing number of excitations, we choose the 3D configuration for this experiment. The results are shown in Fig. 4(a). In this figure, three stages can clearly be distinguished: the initial *seed* or *nucleation stage* (for $t < 10$ μs) in which N grows slowly due to off-resonant single particle excitations (or "seeds") that are suppressed by a factor $\frac{1}{1+(\Delta/\gamma)^2} \approx 1.4 \times 10^{-3}$ compared to the resonant regime, with N approaching unity towards the end of this stage; the *facilitation stage* (10 μs $< t < 50$ μs) in which the number of excitations grows fast due to successive facilitation starting from seeds created in the nucleation stage; and a *saturation stage* ($t > 50$ μs), in which the dynamics decelerates again due to the finite size of the atomic cloud (this regime is visible in the experimental data but already affected by spontaneous decay, which is not included in the simulations; the lifetime of the $70S$ state is around 150 μs [30]). To clearly demonstrate that the sign of the detuning is crucially important for the facilitation constraint, we repeated the above experiment for $\Delta/2\pi = -19$ MHz [Fig. 4(a); data for $\Delta = 0$ are also shown]. Here, the facilitation condition cannot be fulfilled, and only off-resonant excitation of single Rydberg atoms is possible.

The strong correlations induced by the facilitation constraint are even more clearly visible in the Mandel Q parameter shown in Fig. 4(c). For $\Delta/2\pi = +19$ MHz, Q grows up to 30 μs, becoming large and positive, and then decreases to around 0. This can be understood as follows: In the facilitation regime an excited atom enables the excitation of further atoms, so that small fluctuations in the timing of the first few excitations are amplified, leading to a large value of Q. As the system approaches the saturation stage, the dynamics becomes similar to the blockaded case as no further facilitation is possible, and hence Q decreases. This characteristic behavior of the correlations is a genuine many-body effect and, therefore, absent for negative detuning. As in the case of Fig. 3(d), the fact that Q is not 0, as it should be for a purely Poissonian process, is due to technical noise and, possibly, to facilitation of nearby Rydberg states (a few hundred MHz away in the case of the $70S$ state, with $r_{fac} \approx 2.2$ μm), leading to a positive value of Q.

In summary, we have found experimental evidence suggesting that manifest kinetic constraints govern the dynamics of interacting Rydberg gases. The constraints are a consequence of quantum mechanics, but in the strong dissipation regime studied here the overall dynamics of our system is effectively classical [9,10]. Future experiments could systematically probe the crossover from the incoherent to the coherent regime, giving insight into the role of quantum effects in constrained dynamic relaxation. They could also probe the effect of ergodicity breaking due to kinetic constraints [31] and the emergence of nonequilibrium phase transitions [32]. Furthermore, techniques for spatially resolving Rydberg excitations [33–35] should reveal rich spatial correlations in the dynamics [36], in analogy with dynamic heterogeneity in glasses [2–4]. More generally, our results give a further indication of the broad potential for applying ideas from soft-matter physics to the study of interacting atomic systems.

[1] K. Binder and W. Kob, *Glassy Materials and Disordered Solids: An Introduction to Their Statistical Mechanics* (World Scientific, Singapore, 2011).

[2] L. Berthier and G. Biroli, Rev. Mod. Phys. **83**, 587 (2011).

[3] M. D. Ediger and P. Harrowell, J. Chem. Phys. **137**, 080901 (2012).

[4] G. Biroli and J. P. Garrahan, J. Chem. Phys. **138**, 12A301 (2013).

[5] D. Chandler and J. P. Garrahan, Annu. Rev. Phys. Chem. **61**, 191 (2010).

[6] F. Ritort and P. Sollich, Adv. Phys. **52**, 219 (2003).

[7] J. P. Garrahan and D. Chandler, Phys. Rev. Lett. **89**, 035704 (2002).

[8] A. S. Keys, L. O. Hedges, J. P. Garrahan, S. C. Glotzer, and D. Chandler, Phys. Rev. X **1**, 021013 (2011).

[9] I. Lesanovsky and J. P. Garrahan, Phys. Rev. Lett. **111**, 215305 (2013).

[10] I. Lesanovsky and J. P. Garrahan, Phys. Rev. A **90**, 011603(R) (2014).

[11] M. Hoening, W. Abdussalam, M. Fleischhauer, and T. Pohl, Phys. Rev. A **90**, 021603(R) (2014).

[12] M. Gärttner, K. P. Heeg, T. Gasenzer, and J. Evers, Phys. Rev. A **88**, 043410 (2013).

[13] D. Comparat and P. Pillet, J. Opt. Soc. Am. B **27**, A208 (2010).

[14] R. Löw, H. Weimer, J. Nipper, J. B. Balewski, B. Butscher, H. P. Büchler, and T. Pfau, J. Phys. B: At. Mol. Opt. Phys. **45**, 113001 (2012).

[15] M. Marcuzzi, J. Schick, B. Olmos, and I. Lesanovsky, J. Phys. A: Math. Theor. **47**, 482001 (2014).

[16] J. Sanders, M. Jonckheere, and S. Kokkelmans, Phys. Rev. Lett. **115**, 043002 (2015).

[17] C. Ates, T. Pohl, T. Pattard, and J. M. Rost, Phys. Rev. A **76**, 013413 (2007).

[18] C. Ates, T. Pohl, T. Pattard, and J. M. Rost, Phys. Rev. Lett. **98**, 023002 (2007).

[19] C. Carr, R. Ritter, C. G. Wade, C. S. Adams, and K. J. Weatherill, Phys. Rev. Lett. **111**, 113901 (2013).

[20] H. Schempp, G. Günter, M. Robert-de-Saint-Vincent, C. S. Hofmann, D. Breyel, A. Komnik, D. W. Schönleber, M. Gärttner, J. Evers, S. Whitlock, and M. Weidemüller, Phys. Rev. Lett. **112**, 013002 (2014).

[21] N. Malossi, M. M. Valado, S. Scotto, P. Huillery, P. Pillet, D. Ciampini, E. Arimondo, and O. Morsch, Phys. Rev. Lett. **113**, 023006 (2014).

[22] A. Urvoy, F. Ripka, I. Lesanovsky, D. Booth, J. P. Shaffer, T. Pfau, and R. Löw, Phys. Rev. Lett. **114**, 203002 (2015).

[23] T. F. Gallagher, *Rydberg Atoms* (Cambridge University Press, Cambridge, UK, 1994).

[24] M. M. Valado, M. D. Hoogerland, C. Simonelli, E. Arimondo, D. Ciampini, and O. Morsch, J. Phys.: Conf. Ser. **594**, 012041 (2015).

[25] R. Heidemann, U. Raitzsch, V. Bendkowsky, B. Butscher, R. Löw, L. Santos, and T. Pfau, Phys. Rev. Lett. **99**, 163601 (2007).

[26] R. Gutiérrez, J. P. Garrahan, and I. Lesanovsky, Phys. Rev. E **92**, 062144 (2015).

[27] M. Viteau, P. Huillery, M. G. Bason, N. Malossi, D. Ciampini, O. Morsch, E. Arimondo, D. Comparat, and P. Pillet, Phys. Rev. Lett. **109**, 053002 (2012).

[28] E. Urban, T. A. Johnson, T. Henage, L. Isenhower, D. D. Yavuz, T. G. Walker, and M. Saffman, Nat. Phys. **5**, 110 (2009).

[29] A. Gaëtan, Y. Miroshnychenko, T. Wilk, A. Chotia, M. Viteau, D. Comparat, P. Pillet, A. Browaeys, and P. Grangier, Nat. Phys. **5**, 115 (2009).

[30] I. I. Beterov, I. I. Ryabtsev, D. B. Tretyakov, and V. M. Entin, Phys. Rev. A **79**, 052504 (2009).

[31] M. van Horssen, E. Levi, and J. P. Garrahan, Phys. Rev. B **92**, 100305 (2015).

[32] M. Marcuzzi, E. Levi, W. Li, J. P. Garrahan, B. Olmos, and I. Lesanovsky, New J. Phys. **17**, 072003 (2015).

[33] A. Schwarzkopf, R. E. Shapiro, and G. Raithel, Phys. Rev. Lett. **107**, 103001 (2011).

[34] P. Schauß, M. Cheneau, M. Endres, T. Fukuhara, S. Hild, A. Omran, T. Pohl, C. Gross, S. Kuhr, and I. Bloch, Nature (London) **491**, 87 (2012).

[35] G. Günter, H. Schempp, M. Robert-de-Saint-Vincent, V. Gavryusev, S. Helmrich, C. S. Hofmann, S. Whitlock, and M. Weidemüller, Science **342**, 954 (2013).

[36] D. Petrosyan, M. Höning, and M. Fleischhauer, Phys. Rev. A **87**, 053414 (2013).